MODTRAN-based Retrieval of Aerosol Optical Thickness over Chiba Area from Himawari-8/AHI visible images

Zixuan Xue (1), Nofel Lagrosas (1), Hiroaki Kuze (1)

[1] Center for Environmental Remote Sensing, Chiba University, Chiba, Japan
Email: xuezixuan@chiba-u.jp; nofel@chiba-u.jp; hkuze@faculty.chiba-u.jp

KEY WORDS: Himawari-8, Atmospheric correction, MODTRAN, Aerosol model, Look Up Table.

ABSTRACT: Atmospheric aerosol has a pivotal role in both air-pollution and radiation budget studies. In this paper, we retrieve the spatial distribution of aerosol optical thickness (AOT) over Chiba Area from daytime images of Himawari-8 geostationary satellite. The concurrent data from ground-based measurements are used in the analysis, namely the temporal variation of AOT from a sunphotometer and sky-radiometer located at the Center for Environmental Remote Sensing (CEReS), Chiba University. Also, the information on vertical profiles of aerosols and clouds is obtained from the data of NIES (National Institute for Environmental Studies) lidar operated also on the campus of Chiba University. We employ the MODTRAN (MODerate resolution atmospheric TRANsmission) radiative transfer code for simulating the radiance components that reach the AHI sensor onboard the satellite. The retrieval of AOT is based on look-up tables (LUTs) that are calculated for plausible values of both AOT and the surface reflectance for each of the AHI bands. The choice of aerosol model is optimized with the help of sunphotometer and sky-radiometer data coupled with the surface-based weather and aerosol sampling data. Additional information that is available from the present approach is the influence of thin clouds such as cirrus, since the discrimination of aerosol and cirrus effects is usually a difficult task in most of the atmospheric correction studies. We discuss the seasonal changes of AOT and surface reflectance from the present analysis based on LUTs. It is demonstrated that for each season, the satellite data observed on a clear day with minimum aerosol loading can be used to establish a good reference for the analysis of various satellite data such as MODIS or Landsat to evaluate the AOT distribution over the Chiba area.

1. Introduction

Atmospheric correction is implemented on satellite imagery to retrieve optical parameters by removing atmospheric effects (Guanter et al., 2009). Such a correction is especially crucial in cases where satellite images observed on different conditions are to be compared in a quantitative way. Since aerosol optical thickness (AOT) plays an important role in describing the exchange of radiation between the Earth's surface and atmosphere, the precise monitoring of its spatial and temporal changes is indispensable for better understanding of the influence of both natural and anthropogenic activities (Kuze, 2012).

Generally atmospheric correction approaches can be categorized into two types, namely radiative transfer (RT)-code based physical models (Gao et al., 2006) and in-scene based corrections (Eismann, 2012). One of the greatest challenges of this latter method is the measurement of AOT that can vary both spatially and temporally even under clear-sky conditions. The accuracy of atmospheric correction can be adversely affected by the errors of AOT distribution. The RT-code based method, on the other hand, suffers from the lack of a priori, physical information to perform atmospheric corrections, especially when applied to low spectral resolution, multispectral sensors. Although high resolution satellite images can be useful for obtaining AOT

distribution in wide regions, the lack of accurate knowledge on the optical characteristics of surface reflectance often leads to uncertainties in the retrieval of AOT. Furthermore, the precise choice of the suitable aerosol model is still a difficult task, and few studies have employed visibility-derived AOT estimates for atmospheric correction of satellite images (Wilson et al., 2015).

To address the problems mentioned above, the main objective of the present paper is to propose and test a two-step framework for MODTRAN-based retrieval of AOT exploiting both Himawari-8 visible images and concurrent data from ground-based instruments. We obtain the temporal variation of AOT from a sunphotometer and a sky-radiometer operated at the Center for Environmental Remote Sensing (CEReS), Chiba University. Data from the vertical-looking NIES (National Institute for Environmental Studies) lidar, also operated near CEReS, are employed to check the influence of clouds, since thin clouds such as cirrus can be treated in a mostly similar manner to the analysis of aerosol scattering. We employ the MODTRAN4 code for simulating the radiance components that reach the AHI sensor for reproducing the observed spectra. The most appropriate aerosol model is fixed from the information of ground-based estimation for each observation case. The clear-day image observed in a season is utilized to optimize the reflectance distribution. We can make LUTs pixel-by-pixel over Chiba area for some typical aerosol models to retrieve the AOT distribution.

2. Methodology

2.1 Ground-based and Satellite-based Measurement

We derive the temporal change of AOT based on three-wavelength sunphotometer (368, 500, and 678 nm) data using Lambert-Beer law (Cerqueira et al., 2014), coupled with sky-radiometer (380, 500, and 678 nm) data, under clear-sky conditions. The spectrum of solar radiation at the top of atmosphere can be obtained by the calibration procedure based on the Langley plot (Blumthaler et al., 1997). By removing the influence of ozone absorption $\tau_{\mathrm{O}}(\lambda)$ and Rayleigh scattering $\tau_{\mathrm{R}}(\lambda)$, we can calculate AOT as

$$\tau_{\mathrm{A}}(\lambda) = \frac{\ln I_{\mathrm{c}}(\lambda) - 2\ln d - \ln I(\lambda)}{m(\theta_S)} - \tau_{\mathrm{O}}(\lambda) - \tau_{\mathrm{R}}(\lambda)\,, \tag{1}$$

where I_{c} represents the solar radiation intensity at the top of the atmosphere when the Earth-Sun distance is equal to 1 astronomical unit (AU); I is the solar radiation intensity measured by the sunphotometer, d is the Earth-Sun distance in AU, and m is the air mass that corresponds to the solar zenith angle, θ_S. The value of Ångström exponent (AE) is determined from the wavelength dependence of $\tau_A(\lambda)$, which is then used to estimate the value at 550 nm (required as MODTRAN input) and to constrain the appropriate aerosol model. We also use the aerosol vertical profile obtained from the NIES lidar (532 nm) operated on the campus of CEReS. The pertinent value of lidar ratio has been estimated with the Mie calculation (Cachorro and Salcedo, 1991) based on the sampling data recorded at CEReS (Aminuddin et al., 2018). The data of vertical aerosol profile are employed for checking the temporal variation of both the aerosol extinction coefficient and depolarization property (and hence, the non-sphericity of the scattering particles) (Lagrosas et al., 2019).

We obtain the multi-temporal images of the Himawari-8 geostationary meteorological satellite from the CEReS website. As compared with the observation from the low-Earth orbit such as MODIS or Landsat-8, the advantage of Himawari-8 is the availability of much more frequent data, 10 min for the full disk (Purbantoro et al., 2019). In this study, we focus mainly on the three visible bands of advanced Himawari-8 imager (AHI) centered at 0.47, 0.51, and 0.64 μm, with a high temporal resolution of every 10 min. For each band, pixel-by-pixel values of the observed radiance (L_{obs}) can be calculated from the digital number (DN) values as

$$L_{obs}(\lambda) = \left(0.377358 \times DN(\lambda)\right) - 7.547167\,, \quad (2)$$

while the total albedo value as

$$\rho(\lambda) = 0.001559 \times \ L_{obs}\,, \quad (3)$$

Then, the apparent albedo is obtained as

$$\rho_{ap}(\lambda) = \rho(\lambda)\frac{d^2}{\cos\theta_s}\,, \quad (4)$$

Radiative transfer calculation using the MODTRAN4 code is employed to retrieve AOT from the condition that the simulated radiance agrees with the observed radiance for each band.

2.2 Aerosol model-based retrieval of AOT from MODTRAN

In this study, MODTRAN4 code is used to implement the radiative transfer calculation based on atmospheric models, including three typical aerosol models of rural, maritime and urban models for the boundary layer (Manago and Kuze, 2010). For the atmospheric model needed for the evaluation of Rayleigh scattering, we use the mid-latitude summer model between July and October, and the mid-latitude winter model during the other season. Other input parameters are the time and day of year as well as the observation geometry, namely, the altitude of observer, and latitude/longitude of the surface area. The AOT value for each wavelength is provided from the sunphotometer data at the time of satellite observation. For constructing LUTs, the surface reflectance at each wavelength is assumed to change between 0.05 (water body) and 0.6 (urban area), depending on the pixel location. The major output from the RT calculation is the total radiance expressed as

$$L_{total}(\rho, \bar{\rho}, \tau_{550}) = L_{gd}(\tau_{550}) \times \rho + L_{gi}(\tau_{550}) \times \rho \times \bar{\rho} + L_{pm}(\tau_{550}) \times \bar{\rho} + L_0(\tau_{550})\,, \quad (5)$$

where L_{gd} and L_{gi} represent the radiance reflected from the surface pixel directly and indirectly, respectively; L_{pm} refers to the path/surface-scattered radiance; L_0 is the path radiance from the single and multiple scattering in the atmosphere; ρ and $\bar{\rho}$ are the reflectance of the target pixel and the average reflectance around it, respectively. The values of L_{gd}, L_{gi} L_{pm}, and L_0 can be estimated from the MODTRAN4 simulation.

2.3 Iteration process of AOT retrieval

Algorithm 1: Iteration of AOT retrieval

Input: $\rho, \rho_{ap}, \tau_{550}$
Output: $L_{gd}, L_{gi}, L_{pm}, L_{total}, L_0, \tau_{out}$
Initialize τ_{out} *as empty set*;
for *each* τ *in* $range(0, 1, step\ 0.1)$ **do**
  $MODTRAN(L_{gd}, L_{gi}, L_{pm}, L_{total}, L_0) \leftarrow MODTRAN(\rho, \tau_{550})$;
  if *Band <4* **then**
    $\rho'_{clear} \leftarrow Simulate(L_{total})$;
    $\rho \leftarrow \rho'_{clear}$;
    if *clear-sky image* **then**
      $\tau_{clear} \leftarrow LUTs(\rho)$;
      Append τ_{clear} *to* τ_{out} ;
    else
      $\tau_{turbid} \leftarrow LUTs(\rho)$;
      Append τ_{turbid} *to* τ_{out} ;
    end
  else
    break ;
  end
end
return τ_{out}

As shown in Algorithm 1, first we use the clear-day image observed on a day with small aerosol loading ($\tau_{550} < 0.1$) for the determination of the pixel reflectance in the Kanto area (34.75 - 36.50°N, 139.5 - 141.0°E). When the value of AOT is small, the MODTRAN simulation yields a well-defined relation between L_{total} and ρ. Thus, a reasonable distribution of ρ (i.e., a reflectance map) can be determined from the condition of $L_{obs} = L_{total}$. In order to take the possible change of the ρ distribution into account, we prepare such a clear image for each season. We can construct a LUT to retrieve the AOT for each pixel based on the pixel reflectance distribution. The value of AOT can be obtained from the sunphotometer/sky-radiometer data, together with the most appropriate aerosol model (i.e., wavelength dependence of AOT) for each test image. The application of a similar procedure to Landsat-8 imagery will be useful for investigating how the pixel size affects the accuracy of the atmospheric correction. Also, the availability of Himawari-8 images every 10 min enables the study of bi-directional reflectance distribution function (BRDF) for the urban environment.

3. Results and discussion

In this section, we show the results obtained in each step of our proposed algorithm to implement the atmospheric correction on Himawari-8 images over the Kanto-plane area. All the concurrent data are obtained from the ground-based instruments based at CEReS (35.62°N, 140.10°E), Chiba University, under clear-sky conditions.

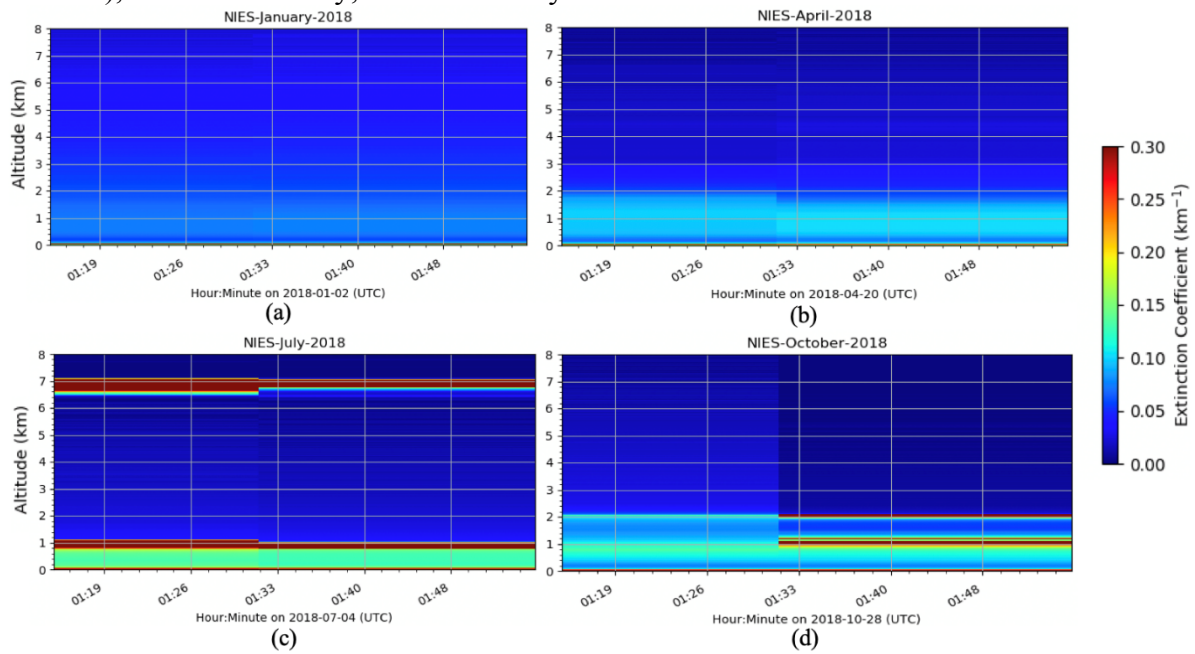

Figure 1 Temporal variation of aerosol extinction coefficient measured by the NIES lidar

Figure 1 shows vertical aerosol profiles observed with the NIES lidar. Panels (a)-(d) show the data observed on January 2, April 20, July 4, and October 28 in 2018, respectively. The observation time is around 10:30 JST, which is 9-h ahead of UTC. The temporal variation of extinction coefficient at 532 nm is seen from the lidar data, which is to be compared with the band-2 data of Himawari-8 (510 nm). As shown in Fig. 1(a), aerosol loading is very small in winter due to the formation of nocturnal boundary layer. Thus, at the surface level, high level air pollution is often reported in winter, including the influence of PM2.5 from anthropogenic emission sources. In spring, higher wind speeds often results in more turbid atmosphere near surface area, as indicated in Fig. 1(b). As shown in Figs. 1(c) and (d), higher aerosol loading in different altitudes occurs in summer and autumn. The effect of hygroscopic growth of aerosol particles is effective in summer because of the high relative humidity. The south wind from the

Tokyo Bay leads to the prevalence of large size, sea salt particles. The existence of a high altitude, thin cloud layer is evident in Fig. 1(c), though no such effect is seen for other cases. In the radiative transfer simulation, such influence of thin cirrus must be removed to properly evaluate the influence of aerosol particles in the lower troposphere.

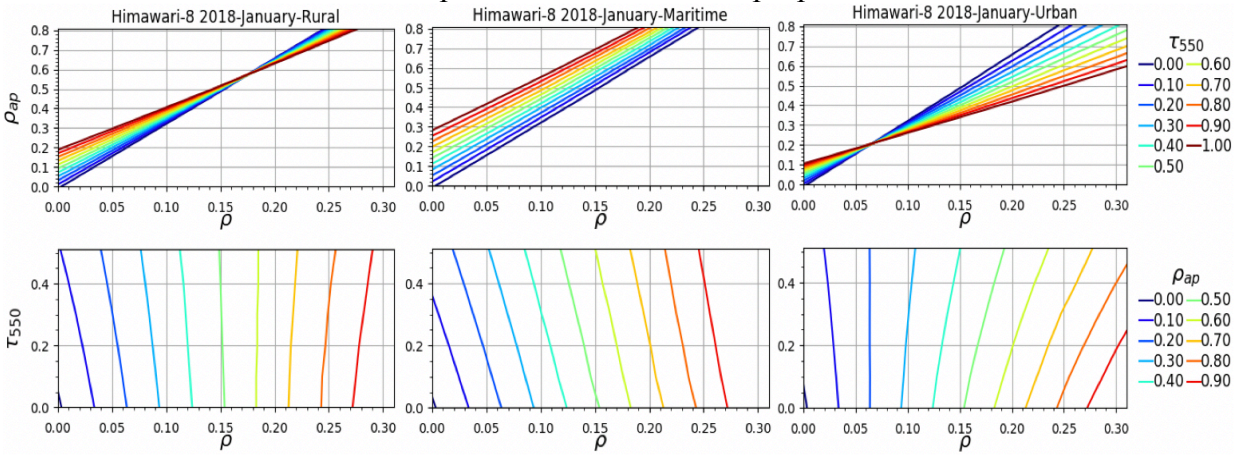

(a) Rural (b)Maritime (c)Urban

Figure 2 LUTs calculated for Himawari-8 band 2 (510 nm) in January 2018. Top panels show the relation between ρ and ρ_{ap}, while bottom panels indicate the relation between ρ and τ_{550}.

Figure 2 shows the comparison among ρ, $\rho_{ap}$and τ_{550} obtained from the MODTRAN4 simulation. Panels (a)-(c) represent the results with rural, maritime, and urban aerosol size distribution models, respectively. The upper panels show the relation between the apparent reflectance (ρ_{ap}) and the surface reflectance (ρ) for various values of AOT at 550 nm (τ_{550}). The lower panels, on the other hand, show the relation between the surface reflectance and AOT at 550 nm for various values of apparent reflectance. The sunphotometer data observed at CEReS is used to constraint the aerosol model through the wavelength dependence of AOT, and we assume this aerosol model can be applied to the whole Kanto area in the first step of our iteration algorithm.

Table 1. Comparison of retrieval AOT values (band 1, January 2 and July 21)

Location	Rural		Maritime		Urban	
	January	July	January	July	January	July
Chiba City	0.24	0.16	0.28	0.14	0.36	0.22
Tokyo Bay	0.16	0.12	0.14	0.08	0.24	0.18

The comparison of values of AOT retrieved at 550 nm is shown in Table 1 for pixels over both the Chiba city area and Tokyo Bay area. The AOT from Himawari-8 varies in the range 0.1-0.4 under relatively clear-sky conditions. The concurrent values from the sunphotometer observation are 0.26 in January and 0.18 in July. Thus, the overall agreement between the results of the ground-based measurement is satisfactory with the values estimated from Himawari-8/AHI, especially under rural and maritime models. The AOT results observed under urban model is larger than the values of maritime model and rural model, which indicates that the urban model is not suitable for analyzing aerosol over the Chiba area. The wind direction is also one of the important factors for AOT loading, especially in winter and summer. Major winds come from northwest direction in winter and southwest direction in summer, transporting aerosols from Tokyo Bay. The AOT values of Tokyo Bay is lower than Chiba City, especially in winter. We have examined the wavelength dependence of AOT, and found the applicability of maritime or rural model for both January and July cases.

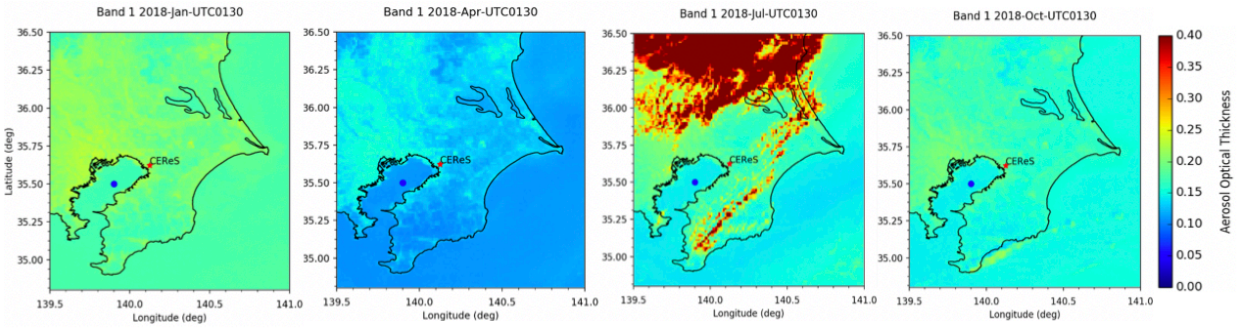

Figure 3 AOT distribution map from Himawari-8. The locations of CEReS and the point over the Tokyo Bay are indicated by dots, where the AOT values in Table 1 have been calculated.

Figure 3 illustrate the AOT distributions retrieved over the Kanto area from Himawari-8 visible images (band 1), assuming aerosol model as maritime and geometrical condition for around 10:30 JST. Panels (a)-(d) are the AOT distributions in January, April, July and October, respectively. The northern part of Fig. 3(c) is covered with cloud, with AOT values exceeding 0.4. This choice of the image is due to the fact that because of the rainy season, the number of clear-sky data are limited from mid-June to late July. Furthermore, the seasonal trend is related to wind directions based on whole year observation over Chiba area. Northwest winds in winter generally cause the dominance of urban aerosols, and southwest winds in summer that of sea salt particles. The seasonal variation of the retrieved AOT indicates the major impacts of sea salt particles in summer, anthropogenic fine particles and dust particles in winter.

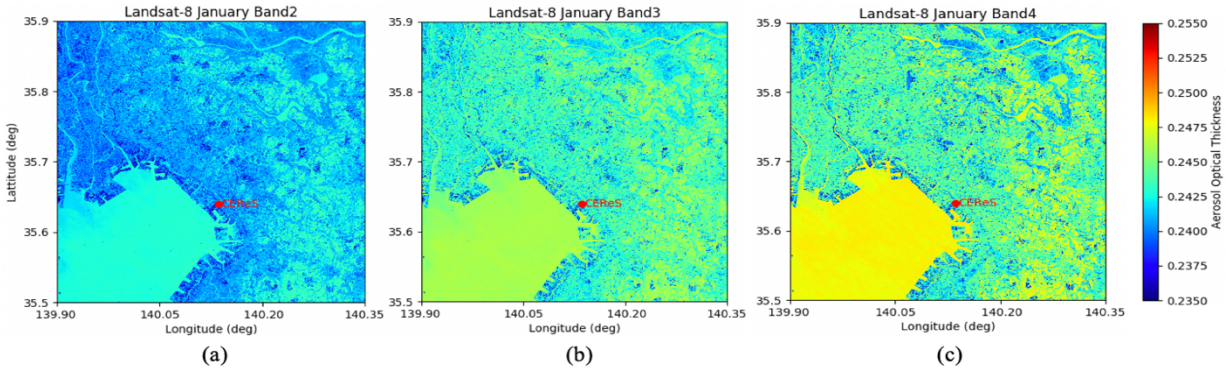

Figure 4 AOT distribution map from Landsat-8 (January 2, 2018).

Figure 4 shows a tentative result of AOT distributions for the visible images from Landsat-8 OLI (Operational Land Imager) observed on January 2, 2018. Although the availability of clear-sky images from Landsat 8 is limited because of its long revisit time (16 days), the fine resolution of its imagery (30 m per pixel) will be useful for dealing with the mixel (mixed pixel) problem inevitable for Himawaru-8 imagery. The AOT from Landsat-8 band 2 (482 nm) varies in the range 0.23-0.25, which reasonably agrees with the result found for Himawari-8 band 1 (470 nm) shown in Fig. 3(a).

4. Conclusion

In this paper, we have described a retrieval method of aerosol optical thickness using LUTs calculated using the MODTRAN4 code. This radiative transfer calculation is based on the choice of different aerosol models. For each season, the satellite data observed on a clear day with minimum aerosol loading can be used to estimate the distribution of surface reflectance needed

for MODTRAN4 simulation over the Kanto area. Such a reference of the surface optical properties, in turn, can be employed to derive the spatial distribution of AOT on both clear and relatively turbid days. In the future work, we aim to optimize the choice of aerosol model, though the maritime or rural model can lead to acceptable results. Also, we demonstrate how the high-temporal resolution imagery from Himawari-8/AHI can be exploited for the detailed study of both Earth surface conditions and AOT distributions. The versatility and reliability of the ground-based measurement is useful for radiation studies, including the validation of satellite data.

References

[1] Aminuddin J., Purbantoro B., Lagrosas N., Manago N., Kuze, H., 2018. Real Time Derivation of Atmospheric Aerosol Optical Properties by Concurrent Measurements of Optical and Sampling Instruments. Open Journal of Air Pollution, 7(02), pp. 140.

[2] Blumthaler, M., Ambach, W., Blasbichler, A., 1997. Measurements of the spectral aerosol optical depth using a sun photometer. Theoretical and Applied Climatology, 57(1-2), pp. 95-101.

[3] Cachorro, V.E., Salcedo L.L., 1991. New improvements for Mie scattering calculations. Journal of Electromagnetic Waves and Applications, 5(9), pp. 913-926.

[4] Cerqueira, J.G., Fernandez J.H., Hoelzemann J.J., et al., 2014. Langley method applied in study of aerosol optical depth in the Brazilian semiarid region using 500, 670 and 870 nm bands for sun photometer calibration. Advances in Space Research, 54(8), pp. 1530-1543.

[5] Eismann, M.T., 2012. Hyperspectral remote sensing. Bellingham : SPIE.

[6] Gao, B.C., Davis C., Geotz A., 2006. A review of atmospheric correction techniques for hyperspectral remote sensing of land surfaces and ocean color. In : IEEE International Symposium on Geoscience and Remote Sensing, USA, pp. 1979-1981.

[7] Guanter, L., Richter R., Kaufmann H., 2009. On the application of the MODTRAN4 atmospheric radiative transfer code to optical remote sensing. International Journal of Remote Sensing, 30(6), pp.1407-1424.

[8] Kuze, H., 2012. Multi-wavelength and multi-direction remote sensing of atmospheric aerosols and clouds. Remote Sensing-Applications, pp. 279-294.

[9] Lagrosas, N., Bagtasa G., Manago N., Kuze, H., 2019. Influence of ambient relative humidity on seasonal trends of the scattering enhancement factor for aerosols in Chiba, Japan. Aerosol and Air Quality Research, pp.1856-1871.

[10] Manago, N., Kuze, H., 2010. Determination of tropospheric aerosol characteristics by spectral measurements of solar radiation using a compact, stand -alone spectroradiometer. Applied Optics, 49(8), pp. 1446-1458.

[11] Wilson, R.T., Milton, E.J., Nield, J.M., 2015. Are visibility-derived AOT estimates suitable for parameterizing satellite data atmospheric correction algorithms. International Journal of Remote Sensing, 36(6), pp. 1675-1688.